Mitigating Electronic Current in Molten Flux for the Magnesium SOM Process

ERIC S. GRATZ, XIAOFEI GUAN, JARROD D. MILSHTEIN, UDAY B. PAL, and ADAM C. POWELL

The solid oxide membrane (SOM) process has been used at 1423 K to 1473 K (1150 °C to 1200 °C) to produce magnesium metal by the direct electrolysis of magnesium oxide. MgO is dissolved in a molten MgF_2-CaF_2 ionic flux. An oxygen-ion-conducting membrane, made from yttria-stabilized zirconia (YSZ), separates the cathode and the flux from the anode. During electrolysis, magnesium ions are reduced at the cathode, and $Mg_{(g)}$ is bubbled out of the flux into a separate condenser. The flux has a small solubility for magnesium metal which imparts electronic conductivity to the flux. The electronic conductivity decreases the process current efficiency and also degrades the YSZ membrane. Operating the electrolysis cell at low total pressures is shown to be an effective method of reducing the electronic conductivity of the flux. A two steel electrode method for measuring the electronic transference number in the flux was used to quantify the fraction of electronic current in the flux before and after SOM process operation. Potentiodynamic scans, potentiostatic electrolyses, and AC impedance spectroscopy were also used to characterize the SOM process under different operating conditions.

DOI: 10.1007/s11663-014-0060-9

I. INTRODUCTION

MAGNESIUM is a leading candidate to replace steel and aluminum in automobiles as magnesium is the least dense structural metal; the density of magnesium is 1.74 g/cm^3, the density of aluminum is 2.80 g/cm^3, and the density of steel ranges from 7.75 to 8.05 g/cm^3. Due to recent increases in oil prices and legislative demand for improved fuel economy, automobile manufacturers are focusing on reducing vehicle weight to increase fuel efficiency.[1] Estimates show that 22.5 kg of automobile mass reduction can improve fuel efficiency by approximately 1 pct.[2]

In order for magnesium to become cost-competitive with steel or aluminum in automobile manufacturing, the cost ratio of magnesium to steel or aluminum must be below a break-even value. Automakers will use magnesium in automobile manufacturing if the magnesium to galvanized steel cost ratio drops below 4.33:1, or the magnesium to aluminum cost ratio drops below 1.8:1. In 2008, the magnesium to galvanized steel cost ratio was 8:1, and the magnesium to aluminum cost ratio was 2.5:1.[3] Magnesium has traditionally been produced by pyro and electro-metallurgical processes,[4] however, new magnesium production methods must be developed in order to decrease the magnesium production cost.

The solid oxide membrane (SOM) process is a new method of metal production in which metal is produced *via* the direct electrolysis of metal oxides, utilizing a SOM.[5,6] In the SOM process, a one-end-closed yttria-stabilized zirconia (YSZ) tube is immersed in a molten fluoride-based flux and separates a liquid metal anode from the flux and cathode. Metal oxide is dissolved in the molten fluoride flux, creating a molten oxy-fluoride melt. When an electric potential is applied across the electrolysis cell, the metal cations are transported to the cathode where they are reduced. Simultaneously, the oxygen anions are transported through the flux and YSZ to the anode where they are oxidized. This electrolysis process is depicted schematically in Figure 1; three possible anode reactions are shown. Magnesium, tantalum, titanium, calcium, and silicon oxides have been reduced to their respective metals *via* the SOM process.[7–12]

In order for magnesium to be produced on a commercial scale by the SOM process, the process must operate for long times with high current efficiencies. A high current efficiency (CE) is required in electrolytic processes for favorable process economics and energy efficiency. At the beginning, for short time periods, the SOM process has been shown to have high current efficiencies approaching 90 pct.[7] As the electrolysis continues, however, the CE of the SOM process drops significantly (CE < 50 pct) due to an electronic current caused by dissolved metal in the flux.[13,14]

Additionally, if the flux has some electronic conductivity, it is possible for the flux to also act as an extended

ERIC S. GRATZ, formerly Graduate Student with the Division of Materials Science and Engineering, Boston University, 15 St. Mary's St., Brookline, MA 02446, is now Post Doctoral Fellow with the Worcester Polytechnic Institute, Worcester, MA. XIAOFEI GUAN, Research Associate, and UDAY B. PAL, Professor, are with the Division of Materials Science and Engineering, Boston University, and also with the Department of Mechanical Engineering, Boston University, 110 Cummington St., Boston, MA 02215. Contact e-mail: upal@bu.edu JARROD D. MILSHTEIN, formerly Graduate Student with the Division of Materials Science and Engineering, Boston University, is now Graduate Student with the MIT, Cambridge, MA. ADAM C. POWELL, Chief Technology Officer, is with Infinium Inc., Natick, MA.

Manuscript submitted November 4, 2013.
Article published online March 29, 2014.

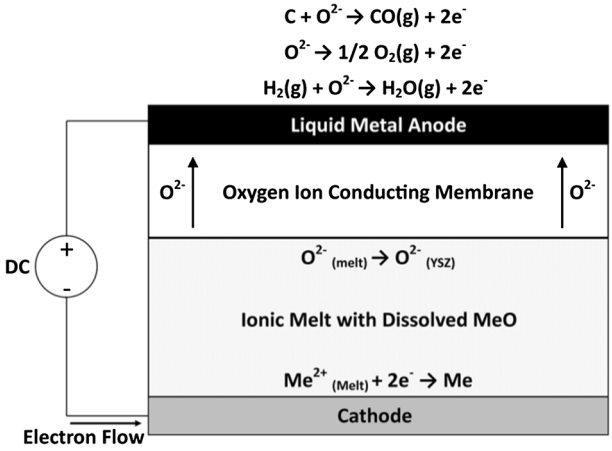

Fig. 1—Schematic of the SOM process for production of a metal (Me) from its oxide.

cathode. In this case, the applied potential reduces the zirconia at the surface of the YSZ membrane to zirconium metal. The YSZ membrane is the lifetime-limiting component of the SOM electrolysis cell.[15] Electrochemical reduction of zirconia in the membrane is one major mechanism for membrane degradation that decreases process lifetime. YSZ is known to be stable in MgF_2-CaF_2 flux containing a small concentration of YF_3, when no potential is applied across the membrane.[15]

As will be shown through theory and experiment in this paper, the fraction of electronic current in the electrolysis cell was decreased by lowering the magnesium partial pressure locally in the flux near the cathode. Three types of electrolysis experiments were performed and compared. First, an experiment with a large cathode area and limited argon stirring in the flux was performed. Second, an experiment with a small cathode area and localized argon stirring in the flux near the cathode was performed. Third, an experiment with a reduced total pressure, small cathode area, and localized argon stirring in the flux near the cathode was performed. The experimental design features of argon stirring in the flux and reduced total pressure were selected to reduce the magnesium partial pressure in the flux and thereby also reduce the amount of soluble magnesium in the flux.

To quantify the electronic current during electrolysis, a method of measuring the electronic and ionic transference numbers of the flux in the SOM electrolysis cell was developed. The transference numbers were measured before and after electrolysis of MgO under different SOM operating conditions. When the electronic transference number was low after electrolysis, the CE was high. Contrastingly, when the electronic transference number was high, the CE was low. The electronic transference number was lowest when electrolysis was operated at reduced total pressure, and this low-pressure experiment resulted in the highest CE. Further, when the electronic transference number was sufficiently low, electrochemical reduction of zirconia in the membrane was not observed.

II. EXPERIMENTAL

A. *Flux Composition*

The flux was comprised of a eutectic mixture of MgF_2-CaF_2 with 2.0 wt pct YF_3 and 10 wt pct MgO.[16] MgF_2 hydrate was purchased (Alfa Aesar) and dried at 573 K (300 °C) for 12 hours to remove the moisture from the salt. 96 pct pure MgO (Alfa Aesar), 99.5 pct pure CaF_2 (Alfa Aesar), and 99.99 pct pure YF_3 were also purchased (Alfa Aesar) and dried for 12 hours at 423 K (250 °C). After drying, the powders were mixed on a ball mill at 200 rpm for 2 hours in the desired proportions. Once the powders had been mixed, the flux was prepared by melting the mixed powders in a graphite crucible at ~1473 K (1200 °C) in a 95 pct argon and 5 pct hydrogen atmosphere. After the flux was cooled to room temperature, it was crushed. 450 g of flux was used in each electrolysis experiment. The density of the flux at 1463 K (1190 °C) was approximately 3.0 g/cm^3.[17]

B. *SOM Electrolysis Cell Designs*

1. *Standard experimental setup*

Figure 2 shows the front-view schematic for a single-tube SOM electrolysis cell used in electrolysis experiments. Figure 3 shows the right-view schematic of the upper reaction chamber of the experimental setup. The setup contained an upper reaction chamber, where magnesium vapor was produced, and a lower condensing chamber, where magnesium vapor was condensed and collected. The electrolysis cell was manufactured from type 304 stainless steel. Stainless steel parts were welded together to ensure vacuum grade sealing.

All electrolysis experiments were performed using a new, as-received, one-end-closed YSZ tube (McDanel Ceramics). The YSZ tubes had a 1.27-cm inner diameter, were 30.48 cm long, and contained 10.5 wt pct yttria. Liquid tin functioned as the anode inside the one-end-closed YSZ tube. The anode had a surface area of 11 cm^2. The anode current collector was a molybdenum tube. Hydrogen gas was bubbled into the liquid tin at 30 cm^3/min, through the molybdenum current collector. The reaction chamber was used as the cathode where magnesium cations were reduced. The overall cell reaction when a molybdenum current collector was used with hydrogen gas is given in Eq. [1].

$$MgO + H_{2(g)} = Mg_{(g)} + H_2O_{(g)} \qquad [1]$$

An isolated argon stirring tube was used as an alternate electrode. The transference numbers in the flux between the alternate electrode and the reaction chamber cathode were determined by a method that is described in Section III–D of this paper.

The reaction chamber contained the flux and was connected to the condensing chamber by two stainless steel tubes. The reaction chamber was maintained in the temperature range of 1423 K to 1473 K (1150 °C to 1200 °C). Industrial grade argon gas (Airgas) was passed through the annulus between the YSZ tube and the stainless steel tube extending out of the top of the

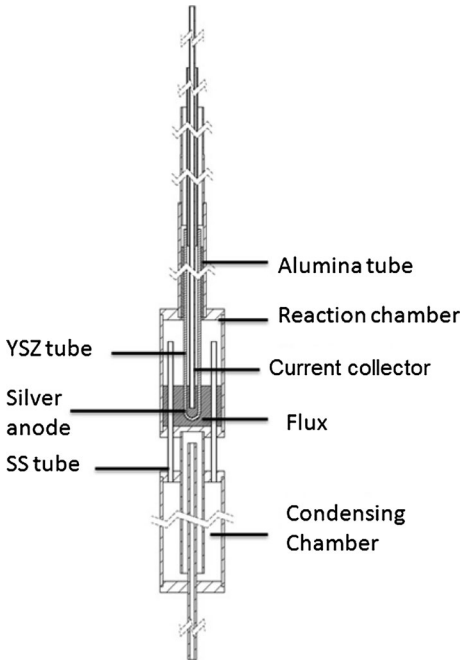

Fig. 2—Front view of a standard single-tube SOM electrolysis cell. Isolated stirring tube is not shown.

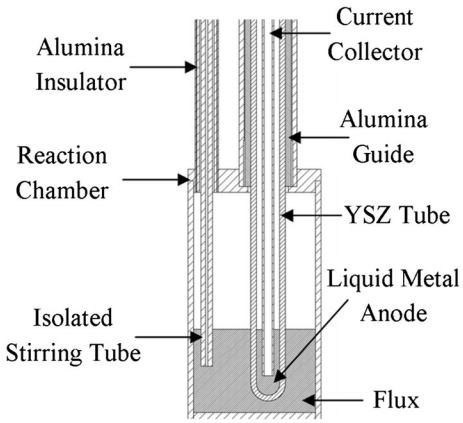

Fig. 3—Right view of reaction crucible design with an isolated stirring tube electrode.

electrolysis cell. The argon gas was purified before it entered the electrolysis cell; it was first passed through a drierite trap to remove water vapor and second through a magnesium trap heated to 673 K (400 °C) to remove oxygen. The maximum P_{O_2} of the argon gas after passing through the two purifying traps was measured with a zirconia-based [at 973 K (700 °C)] oxygen sensor to be less than 10^{-17} atm. During electrolysis, the argon gas carried magnesium vapor produced in the reaction chamber through the two stainless steel tubes, depicted in Figure 2, into the condensing chamber. The argon carrier gas flow rate was 300 cm^3/min. The condensing chamber was maintained in the temperature range of 1373 K to 573 K (1100 °C to 300 °C), and magnesium vapor was collected on a stainless steel shim placed along the side walls of the condensing chamber.

The SOM electrolysis cell exterior was maintained in a reducing atmosphere of 95 pct argon, 5 pct hydrogen (Airgas) to prevent oxidation of the stainless steel. To maintain this low P_{O_2} environment, the electrolysis cell was sealed inside a mullite tube (9.53 cm inner diameter), using brass compression fitting end caps. The mixture of 95 pct argon and 5 pct hydrogen was passed through the annulus between the electrolysis cell and the mullite tube. Swagelok Ultra-Torr vacuum fittings were used to connect the brass compression fitting to the gas lines entering the electrolysis cell, providing an air-tight seal.

The electrolysis cell was heated to the aforementioned operating temperatures in a tube furnace at a rate of 4 °C/min. During electrolysis cell heating, the closed end of the YSZ tube was 2.54 cm above the top of the flux. Once the experimental setup reached the operating temperature, the YSZ tube was lowered into the flux at 0.25 cm/min until the closed end of the YSZ tube was suspended 0.64 cm above the bottom of the reaction chamber.

Figure 3 shows a right-view schematic of the reaction chamber design, which houses an isolated argon stirring tube electrode. The 0.64-cm-outer diameter stirring tube was passed down the annulus of a 0.84-cm-inner diameter alumina tube. The alumina tube was contained in a 1.14-cm-inner diameter stainless steel tube which was welded to the top of the reaction chamber; the alumina tube provided electrical insulation, isolating the argon stirring tube electrode from the electrolysis cell wall. Again, the stirring tube was immersed into the flux, 2.54 cm above the bottom of the reaction chamber, and argon was stirred into the flux at 150 cm^3/min. The surface area of the stirring tube in the flux was estimated to be 7.1 cm^2.

2. *Inert anode current collector*

An electrolysis experiment employing isolated stirring tube as the cathode was performed with an inert anode current collector. The molybdenum current collector was replaced with an inert LSM ($La_{0.8}Sr_{0.2}MnO_3$)—Inconel current collector submerged in an inert liquid silver anode, as shown in Figure 4. The reaction chamber was used as an alternate electrode to determine transference numbers in the flux. When the inert anode current collector was used, the overall cell reaction is given by Eq. [2].

$$MgO = Mg_{(g)} + \frac{1}{2}O_{2(g)} \quad [2]$$

The effect of lower MgO content and argon flow rate was investigated using an inert anode current collector. Flux composition and the argon flow rate used are outlined below:

1. Flux composition: 5 wt pct MgO, 2 wt pct YF_3, and 93 wt pct eutectic mixture of MgF_2-CaF_2.
2. Argon stirring rate: 125 cm^3/min.

3. *Reduced pressure setup*

A SOM electrolysis experiment was performed at a total pressure of 8106 Pa (0.08 atm) in the reaction as well as the condensing chambers. Operating temperatures

were the same as previously described. In reduced pressure experiments, the pressure inside the YSZ tube was maintained 133 to 266 Pa (1 to 2 Torr) below the pressure of the reaction chamber, preventing oxygen or water vapor from leaking into the reaction chamber. A schematic of the reduced pressure setup is shown in Figure 5.

In the reduced pressure design, the reaction chamber was identical to the schematic shown in Figure 3, and the cathode was the isolated argon stirring tube electrode. A liquid tin anode was specifically used due to its lower vapor pressure when compared to that of silver.[18,19] A molybdenum tube current collector was submerged in the liquid tin, and hydrogen gas was bubbled through the molybdenum tube at 30 cm^3/min.

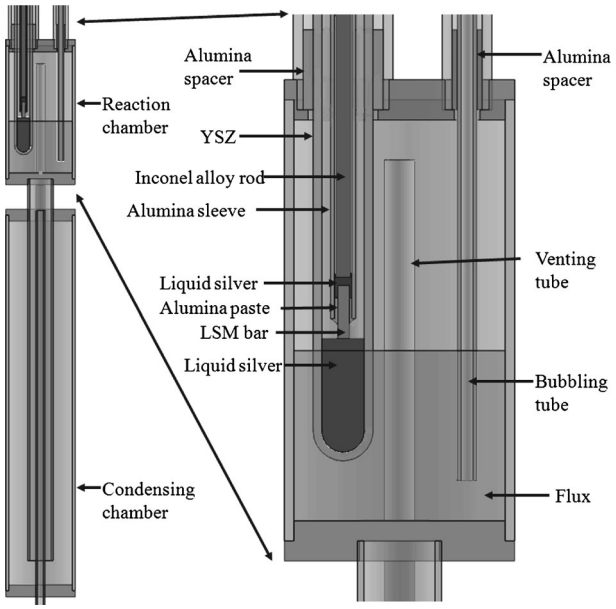

Fig. 4—Right view of the SOM electrolysis cell design with an inert anode current collector.

Purified industrial grade argon was passed as before, through the annulus between the YSZ tube and the stainless steel tube extending out of the top of the electrolysis cell, but at a decreased flow rate of 147 cm^3/min. Argon was also passed through the annulus between the stirring tube and alumina insulator at 60 cm^3/min to prevent backward flow of argon gas in this region. To compensate for the reduced pressure, argon was stirred into the flux, through the stirring tube, at a decreased rate of 15 cm^3/min.

C. *Electrochemical Characterization*

Electrochemical measurements were performed using one of the three following instruments: 1) Princeton Applied Research 263A potentiostat, 2) Solartron 1250 frequency response analyzer, or 3) Agilent Technologies N5743A power supply. AC impedance spectroscopy was used to determine the ohmic resistance of the electrolysis cell and flux[17]; impedance scans were performed from 5000 to 0.1 Hz with 10 mV amplitude. Before electrolysis experiments were performed, potentiodynamic scans (PDS) were performed at a scan rate of 5 mV/s in order to determine the dissociation potential of MgO and to measure the leakage current before MgO dissociation. Electrolysis experiments were then performed by applying constant DC potentials greater than the measured dissociation potential of MgO. Electrolysis experiments lasted between 1 and 4 hours. Open circuit voltage (OCV) measurements were taken before and after electrolysis experiments.

In some experiments, the anode effluent gas flow rate was measured during electrolysis to assist in calculating the cell current efficiency. Anode effluent gas flow rate was measured by passing the gas through an Omega Engineering FMA-4305 digital flow meter. It is important to note that the mass flow rate of the anode effluent gas could not be measured until oxygen which had dissociated from MgO saturated the liquid metal anode. Typically, the system reached a steady-state anode

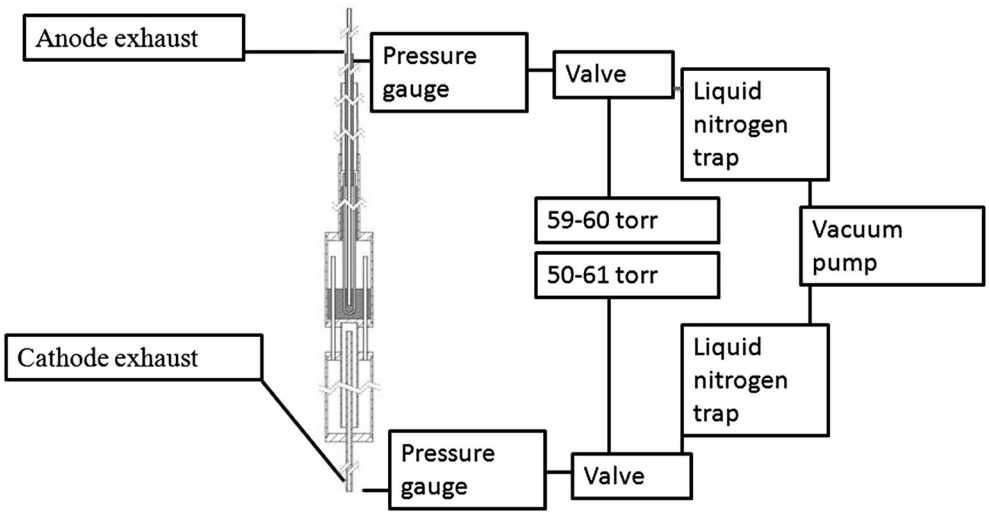

Fig. 5—Flow chart of the reduced total pressure electrolysis apparatus.

effluent gas flow rate within 10 minutes to 1 hour of beginning an electrolysis experiment.

III. THEORETICAL

A. *Current Efficiency*

The CE of the SOM electrolysis is defined as the percentage of total current involved in producing magnesium metal. CE is defined in Eq. [3], where $\frac{dN_{Mg}}{dt}$ is the molar rate of magnesium metal production, F is Faraday's constant, and I is the total current through the electrolysis cell. CE can be determined in a straightforward manner from the total current passed through the cell and the molar rate of magnesium metal production.

$$\text{CE} = \frac{dN_{\text{Mg}}}{dt} \cdot \frac{2F}{I} \qquad [3]$$

Depending on the current collector used at the anode of the SOM process, carbon monoxide, water vapor, or oxygen evolved at the anode. From the reaction stoichiometry, the rate of anode gas production can be directly related to the molar rate of production of magnesium metal in Eq. [3]. Thus, the CE can also be calculated from the rate of gas evolved at the anode and the current passing through the electrolysis cell.

B. *Magnesium Solubility in the Flux*

As has been previously reported by the authors, after SOM electrolysis is performed using the reaction chamber wall as the cathode and the cell is cooled at 4 °C/min, dissolved metal is detected in the flux at room temperature by exposing the flux to hydrochloric acid and measuring the volume of gas produced.[13,14] Assuming that the dissolved metal was magnesium, the metal–acid reaction is given in Eq. [4]. From the volume of gas evolved during the reaction, it was estimated that 0.02 to 0.05 wt pct magnesium metal dissolves in the flux.[12,13]

$$\text{Mg}_{(\text{flux})} + 2\text{HCl}_{(\text{aq})} = \text{MgCl}_{2(\text{s})} + \text{H}_{2(\text{g})} \qquad [4]$$

The solubility of magnesium in MgF_2 has been reported to be between 0.3 and 0.6 mol pct (0.12 to 0.23 wt pct) at 1534 K (1261 °C), which is the melting point of MgF_2.[20] The solubility of metals in salts is highest in salts of their own cation.[20] Therefore, it is believed that pure MgF_2 will have a higher solubility of magnesium metal than the MgF_2-CaF_2 eutectic mixture.[21–23] The dissolved metal concentration measured after electrolysis may possibly also be smaller than the dissolved metal concentration during SOM electrolysis, because the system was slowly cooled (4 °C/min) and the metal solubility was measured at room temperature. It is possible that some magnesium metal was removed from solution during the cooling process.

Dissolved metal in the flux is believed to be the source of the electronic conductivity in the flux. Dissolved metal has been shown to decrease CE and increase electronic conductivity for electrolysis processes involving several different molten salt mixtures.[24] Specifically in prior studies of the SOM process, it was found that calcium dissolved in a molten CaF_2-$CaCl_2$ flux at 1023 K (750 °C). The dissolved calcium metal was the source of electronic conductivity in the flux in the SOM process for calcium production.[10,25] Additionally, the solubility of magnesium metal in MgF_2-CaF_2 mixtures has been exploited to recycle magnesium alloys.[26–28] By comparing conclusions drawn in available literature, the dissolved metal in the flux described in this paper is believed to be magnesium and is the source of the electronic current.

C. *SOM Equivalent Circuit*

An equivalent circuit of the SOM electrolysis cell was developed to determine the impact of electronic conductivity in the flux, and this equivalent circuit is shown in Figure 6. The symbols used in Figure 6 are defined in Table I. In the equivalent circuit, impurity oxides with greater cation electronegativity than magnesium (such as Fe_2O_3) will dissociate before MgO. After the impurity cations are reduced at the cathode, the magnesium cations are reduced. Some of the reduced magnesium can dissolve in the flux. The dissolved magnesium subsequently increases the electronic conductivity of the flux. A flux with electronic conductivity allows for electronic current to pass through the flux and membrane, decreasing the CE. If the flux had no electronic conductivity, then the current passing through the flux would be purely ionic, and all of the energy input to the cell would be used in the process for dissociating MgO. The presence of an electronic current acts as an internal short in the SOM process.

As more magnesium dissolves into the flux, the electronic conductivity of the flux will further increase. The increased electronic conductivity also decreases the potential drop across the flux, and then the potential drop across the YSZ membrane must necessarily increase while a constant DC potential is applied across the entire cell. The increased potential drop across the YSZ can cause the dissociation of zirconia, which will degrade the YSZ membrane. Further, as the electronic conductivity increases, the total resistance decreases, and the total current will increase at any given applied

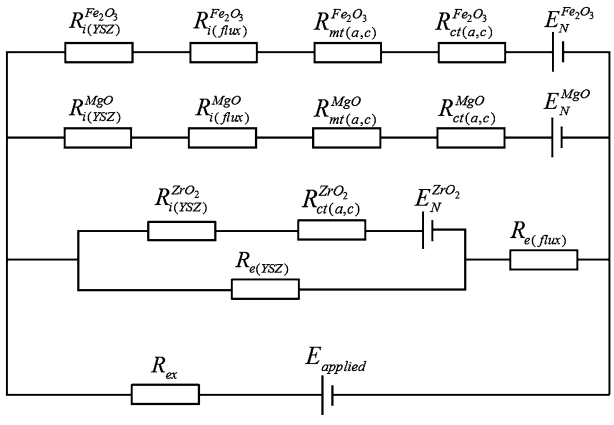

Fig. 6—Equivalent circuit of the SOM process for magnesium production.

Table I. Definitions of Symbols in the SOM Equivalent Circuit, Which is Shown in Fig. 6

Symbol	Definition
$R_{i(\mathrm{YSZ})}^{\mathrm{Fe_2O_3}}$	ionic resistance of YSZ membrane involved for Fe_2O_3 dissociation
$R_{i(\mathrm{YSZ})}^{\mathrm{MgO}}$	ionic resistance of YSZ membrane involved for MgO dissociation
$R_{i(\mathrm{YSZ})}^{\mathrm{ZrO_2}}$	ionic resistance of YSZ membrane involved for ZrO_2 dissociation
$R_{i(\mathrm{flux})}^{\mathrm{Fe_2O_3}}$	ionic resistance of flux involved for Fe_2O_3 dissociation
$R_{i(\mathrm{flux})}^{\mathrm{MgO}}$	ionic resistance of flux involved for MgO dissociation
$R_{\mathrm{mt}(a,c)}^{\mathrm{Fe_2O_3}}$	mass transfer resistance at the anode and cathode for Fe_2O_3 dissociation
$R_{\mathrm{mt}(a,c)}^{\mathrm{MgO}}$	mass transfer resistance at the anode and cathode for MgO dissociation
$R_{\mathrm{ct}(a,c)}^{\mathrm{Fe_2O_3}}$	charge transfer resistance at the anode and cathode for Fe_2O_3 dissociation
$R_{\mathrm{ct}(a,c)}^{\mathrm{MgO}}$	charge transfer resistance at the anode and cathode for MgO dissociation
$R_{\mathrm{ct}(a,c)}^{\mathrm{ZrO_2}}$	charge transfer resistance at the anode and cathode for ZrO_2 dissociation
$R_{\mathrm{e,(YSZ)}}$	electronic resistance of the YSZ membrane
$R_{\mathrm{e,(flux)}}$	electronic resistance of the flux
R_{ex}	resistance of external circuit elements
$E_{\mathrm{N}}^{\mathrm{Fe_2O_3}}$	Nernst potential for Fe_2O_3 dissociation
$E_{\mathrm{N}}^{\mathrm{MgO}}$	Nernst potential for MgO dissociation
$E_{\mathrm{N}}^{\mathrm{ZrO_2}}$	Nernst potential for ZrO_2 dissociation
E_{applied}	applied potential

potential resulting in a higher potential drop in the leads and contacts. Therefore, the applied potential across the entire cell required for MgO dissociation will need to be increased. These observations were noted during the SOM electrolysis experiments.

D. *Measuring Transference Numbers*

As previously stated, it is believed that the flux becomes electronically conductive due to the presence of dissolved magnesium in the flux. Measuring the electronic and ionic transference numbers in the flux can reveal more information regarding the role of dissolved magnesium in imparting electronic conductivity on the flux. When the flux has both electronic and ionic conductivity, the total ohmic resistance due to the flux can be modeled as two resistors in parallel, where one resistor represents the electronic resistance, and the second resistor represents the ionic resistance.

The isolated argon stirring tube electrode cell design, shown in Figure 3, was employed to determine the transference numbers in the flux. A small AC potential was applied between the reaction chamber wall and the isolated argon stirring tube. The impedance between these two stainless steel elements was then measured as a function of frequency. Nyquist plots were produced to plot the negative imaginary part of the impedance against the real part of the impedance as a function of frequency; the high-frequency intercept on the real axis of the Nyquist plot corresponds to the total ohmic resistance, R_{tot}, of the flux.[29,30]

The total ohmic resistance of the flux can be modeled as electronic and ionic resistances in parallel. The total ohmic resistance of the flux can be calculated using Eq. [5], where R_{e} is the ohmic electronic resistance in the flux and R_{ion} is the ohmic ionic resistance in the flux.

$$R_{\mathrm{tot}} = \frac{R_{\mathrm{e}} \cdot R_{\mathrm{ion}}}{R_{\mathrm{e}} + R_{\mathrm{ion}}} \quad [5]$$

The ohmic electronic resistance, R_{e}, can be determined experimentally by applying a DC potential (~0.1 V) that is less than the dissociation potentials of MgO and impurity oxides between the reaction chamber wall and the isolated argon stirring tube electrode. The current, at steady state, between the reaction chamber wall and isolated argon stirring tube is believed to be purely electronic current.[31] Ohm's law was used to calculate R_{e} from the measured current and the magnitude of the applied DC potential. The measured values of R_{tot} and R_{e} were used to calculate the electronic and ionic transference numbers as described in the following paragraphs.

The total current passing through the cell is the sum of the electronic and ionic currents. Subsequently, the summation of the electronic and ionic transference numbers must be equal to 1, as demonstrated in Eq. [6], where t_{e} is the electronic transference number, and t_{ion} is the ionic transference number.[32]

$$t_{\mathrm{e}} + t_{\mathrm{ion}} = 1 \quad [6]$$

The electronic transference number is the ratio of the electronic conductivity to the total conductivity, as shown in Eq. [7], where σ_{e} is the electronic conductivity, and σ_{tot} is the total conductivity.

$$t_{\mathrm{e}} = \frac{\sigma_{\mathrm{e}}}{\sigma_{\mathrm{tot}}} \quad [7]$$

Similarly, the ionic transference number is the ratio of the ionic conductivity to the total conductivity, as shown in Eq. [8], where σ_{ion} is the ionic conductivity.

$$t_{\mathrm{ion}} = \frac{\sigma_{\mathrm{ion}}}{\sigma_{\mathrm{tot}}} \quad [8]$$

The electronic conductivity is proportional to the inverse of electronic resistance, and the ionic conductivity is proportional to the inverse of ionic resistance.[33] Since the cell constant during the measurements does not change for electronic and ionic species, the electronic transference number and ionic transference number can be written as shown in Eqs. [9] and [10], respectively.

$$t_{\mathrm{e}} = \frac{R_{\mathrm{ion}}}{R_{\mathrm{ion}} + R_{\mathrm{e}}} \quad [9]$$

$$t_{\mathrm{ion}} = \frac{R_{\mathrm{e}}}{R_{\mathrm{ion}} + R_{\mathrm{e}}} \quad [10]$$

Equation [5] can be rearranged into Eq. [11] to write R_{ion} as a function of R_{e} and R_{tot}.

$$R_{ion} = \frac{R_{tot} \cdot R_e}{R_e - R_{tot}} \quad [11]$$

Finally, Eq. [11] can be substituted into Eqs. [9] and [10] to solve for the electronic and ionic transference numbers as functions of the experimentally determined variables, R_e and R_{tot}, as shown in Eqs. [12] and [13].

$$t_e = \frac{R_{tot}}{R_e} \quad [12]$$

$$t_{ion} = \frac{R_e - R_{tot}}{R_e} \quad [13]$$

E. *Effect of Magnesium Partial Pressure*

At 1473 K (1200 °C), magnesium is produced as a vapor at the cathode and begins to equilibrate with the flux according to the reaction shown in Eq. [14].

$$Mg_{(g)} = Mg_{(flux)} \quad [14]$$

The equilibrium constant for the reaction can be presented according to Eq. [15], where K_d is the equilibrium constant of the dissolution reaction, γ is the activity coefficient of dissolved magnesium in the flux, $[Mg_{(flux)}]$ is the concentration of magnesium dissolved in the flux, $P_{Mg_{(cathode)}}$ is the partial pressure of magnesium vapor near the cathode, and P^0_{Mg} is the vapor pressure of pure magnesium at 1463 K (1190 °C).

$$K_d = \frac{\gamma\left[Mg_{(flux)}\right]}{\left(\frac{P_{Mg_{(cathode)}}}{P^0_{Mg}}\right)} \quad [15]$$

According to Eq. [15], by lowering the partial pressure of magnesium near the cathode, the concentration of magnesium in the flux should decrease. Decreasing the concentration of magnesium in the flux will then decrease the electronic conductivity of the flux. SOM experiments with argon stirring near the cathode were intended to demonstrate this concept, because the argon gas present in the flux decreases the magnesium partial pressure near the cathode.

By lowering the total pressure above the flux, the magnesium partial pressure in the flux can also be decreased and subsequently, the concentration of magnesium dissolved in the flux will decrease, as demonstrated by Eq. [15]. A SOM electrolysis experiment was performed with reduced total pressure to demonstrate this concept.

F. *Leakage Current*

In an ideal SOM electrolysis cell, no current should pass through the cell at applied potentials less than the dissociation potential of MgO because dissociated Mg^{2+} and O^{2-} ions are the only species in the flux intended to carry current through electron transfer reactions at the electrodes. However, prior research on the SOM process for magnesium production has shown that under certain conditions a small current is observed when a DC potential less than the dissociation potential of MgO is applied across the electrolysis cell.[7] This current is referred to as the leakage current.

It was previously reported that the leakage current can be caused by impurity oxygen in the argon (10 ppm in industrial grade argon, $PO_2 = 10^{-5}$ atmospheres) entering the electrolysis cell.[7] The reduction of impurity oxygen to oxide ions at the cathode and the corresponding oxidation of the oxide ions at the anode results in the leakage current from oxygen impurity. However, the magnesium vapors during electrolysis will getter most of this impurity oxygen bringing the PO_2 to less than 10^{-33} atmospheres and thus will lower the leakage current from impurity oxygen to negligible level with virtually no impact on the yield for magnesium production. Through more recent work, however, it is now understood that the leakage current is also caused by impurity oxides and magnesium metal dissolved in the flux. As previously described, impurity oxides in the flux with higher cation electronegativity than magnesium will dissociate at applied potentials lower than the dissociation potential of MgO, carrying current at lower potentials. Also, as is the focus of this paper, dissolved magnesium metal imparts some electronic conductivity in the flux, allowing current to flow at any applied potential. Thus, the leakage current is defined by the sum of currents imparted by the reduction of impurity oxygen, the dissociation of impurity oxides of cations with higher electronegativities, and the electronic current due to dissolved magnesium; the focus of this paper is on the last contribution.

When leakage current was present prior to an electrolysis experiment, the leakage current was due to only impurity oxygen and impurity oxides; no magnesium metal was yet produced to dissolve in the flux and carry electronic current. In this scenario, the leakage current could typically be reduced by applying a DC potential, lower than the dissociation potential of MgO, to remove impurity oxygen and impurity oxides. This technique was employed in some of the SOM experiments described, and this technique will be noted when employed in a given experiment.

G. *Open Circuit Voltage (OCV)*

Before and after SOM electrolysis experiments, an OCV was generated due to difference in oxygen partial pressure between the liquid metal anode and the cathode. The OCV can be represented by the Nernst potential equation shown in Eq. [16], where R is the gas constant, T is temperature, t_{ion} is the ionic transference number, $P_{O_2,\,anode}$ is the oxygen partial pressure at the anode, and $P_{O_2,\,cathode}$ is the oxygen partial pressure at the cathode.[34] Since the oxygen potential at the cathode is determined by Mg/MgO equilibrium, the OCV measurements were used in some experiments to gather

information regarding the magnesium partial pressure (solubility) in the flux, as will be described.

$$E_{OCV} = t_{ion}\frac{RT}{4F}\ln\left(\frac{P_{O_2,\,anode}}{P_{O_2,\,cathode}}\right) \quad [16]$$

H. *Zirconia Reduction*

The standard Nernst potentials for zirconium dioxide (ZrO_2 or zirconia) and MgO dissociations were calculated using Eq. [17], and the values are shown in Table II. In Eq. [17], E°_{rxn} is the standard Nernst potential, ΔG°_{rxn} is the standard Gibbs free energy change of the reaction, n is the number of charge carriers, and F is Faraday's constant. The standard Gibbs free energy change values were obtained from HSC 5.1™ Database.[35]

$$E^{\circ}_{rxn} = \frac{-\Delta G^{\circ}_{rxn}}{nF} \quad [17]$$

As shown in Table II, the reduction of ZrO_2 is more favorable than the reduction of MgO at 1473 K (1200 °C), assuming that both species behave ideally and given the same anode conditions in the SOM process. During the SOM process, the YSZ membrane is protected from electrochemical ZrO_2 reduction due to the electronic potential drop across the flux. Even when the flux has some electronic conductivity, the electronic potential drop across the flux is such that the zirconia does not experience most of the applied potential drop across the entire electrolysis cell. But, if the electronic conductivity in the flux and the applied potential across the electrolysis cell are both sufficiently high, then the potential drop across the YSZ membrane can be large enough to dissociate the zirconia. The mechanism of reduction is not completely understood, but it is believed that the zirconia at the interface of the flux and YSZ membrane is reduced to a ZrO_{2-x} species which enters the flux. The zirconia species is then fully reduced to zirconium metal at the cathode while oxygen ions are oxidized at the anode.

IV. RESULTS AND DISCUSSION

This section aims to summarize the results of the SOM experiments performed as well as discuss noteworthy observations and conclusions from those experiments. Details of the SOM experiments are provided in tabular format (Tables III, IV, V), with row headings as defined in the following list:

(a) *PDS range* Potential range scanned prior to the potentiostatic electrolysis.
(b) *Leakage current* The leakage current measured at an applied potential lower than the dissociation potential of MgO. For comparison, the potential of 0.5 V was chosen during the PDS.
(c) *Dissociation potential* The minimum required applied potential to dissociate MgO determined by the PDS.
(d) *Electrolysis potential* Magnitude of the applied constant DC potential during electrolysis.
(e) *Electrolysis duration* Duration of the potentiostatic electrolysis.
(f) *Coulombs passed* Amount of total charge passed through the electrolysis cell, measured in Coulombs (C).
(g) *Steady-state CE* The current efficiency at steady state; the current efficiency was measured *in situ* during SOM experiments.
(h) *Total pressure* The total pressure inside the SOM electrolysis cell during the electrolysis experiment.

A. *Reaction Chamber Wall Cathode*

An experiment was performed to determine the electronic and ionic transference numbers before and after electrolysis; electrolysis details are shown in Table III. The SOM electrolysis cell design shown in Figure 3 was employed; the reaction chamber wall was maintained as the cathode while the isolated argon stirring tube acted as an alternate electrode.

The electronic transference number upon heating the electrolysis cell to the operating temperature was measured to be 0.02. A 0.56-V DC potential was then applied

Table III. Electrolysis Details from Experiment Using the Standard Experimental Setup

	Electrolysis 1
PDS range (V)	0.4 to 1.8
Leakage current density before electrolysis (A/cm^2)	<0.03
Dissociation potential (V)	1.2
Electrolysis potential (V)	1.7
Electrolysis duration (h)	2
Coulombs passed (C)	13987
Total pressure (atm)	1

Reaction chamber wall was the cathode.

Table II. Standard Nernst Potentials for Relevant SOM Reactions

Reaction	Temperature [K (°C)]	ΔG°_{rxn} (kJ)	E°_{rxn} (V)
$MgO = Mg_{(g)} + 1/2O_{2(g)}$	1473 (1200)	429	−2.22
$MgO + H_2 = Mg_{(g)} + H_2O_{(g)}$	1473 (1200)	262	−1.36
$ZrO_2 = Zr + O_{2(g)}$	1473 (1200)	822	−2.13
$ZrO_2 + 2H_{2(g)} = Zr + 2H_2O_{(g)}$	1473 (1200)	489	−1.26

Table IV. Electrolysis Experiment Details from Inert Anode Current Collector Experiment

	Electrolysis 1	Electrolysis 2	Electrolysis 3	Electrolysis 4
Electrolysis potential (V)	2.5	2.4	2.6	2.4
Electrolysis duration (h)	4	4	4	4
Coulombs passed (C)	9,877	8,859	12,985	7,699
Steady-state CE (pct)	90 to 75	75 to 40	50	50
Total pressure (atm)	1	1	1	1

Table V. Electrolysis Experiment Details from Reduced Total Pressure Experiment

	Electrolysis 1	Electrolysis 2	Electrolysis 3
PDS range (V)	0.3 to 1.5	0.8 to 1.4	0.9 to 1.6
Leakage current density (A/cm^2)	<0.02	<0.02	<0.02
Dissociation potential (V)	0.68/1.22	1.22	1.25
Electrolysis potential (V)	1.6	1.7	1.5
Electrolysis duration (h)	4	4.5	3
Coulombs passed (C)	11703	14706	6588
Total pressure (atm)	0.08	0.08	0.24

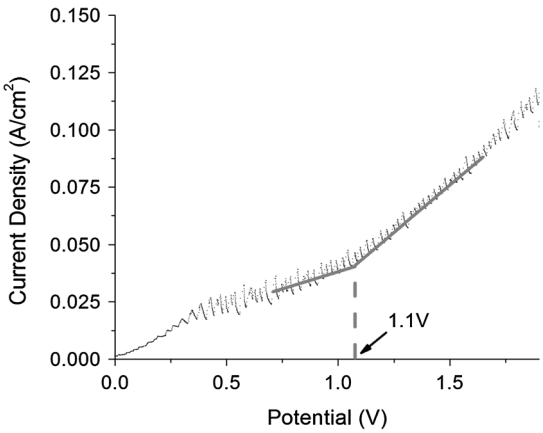

Fig. 7—PDS from reaction chamber wall experiments. The dissociation potential of MgO was identified to be approximately 1.1 V. All PDS were performed after measuring the transport numbers.

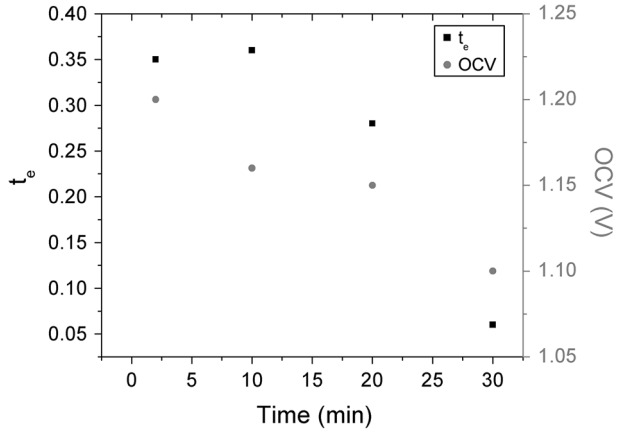

Fig. 8—t_e and OCV as a function of time after reaction chamber cathode electrolysis experiment.

across the electrolysis cell in an attempt to remove any impurity oxygen and impurity oxides from the system. After applying the potential for 10 minutes, t_e was again measured to be 0.02. The overall ohmic resistance of the electrolysis cell, measured between the liquid tin anode and the crucible wall cathode, was 0.57 Ω before any electrolysis was performed. A PDS scan was performed before electrolysis and is shown in Figure 7. The leakage current measured in the scan was less than 0.03 A/ cm^2 at 0.5 V, which agrees with the low electronic transference number measured. The electric potential for MgO dissociation was identified to be approximately 1.1 V at the deflection point of the current–potential curve, as shown in Figure 7. It is close to the absolute value of the standard Nernst potential (1.36 V) for the reaction $MgO + H_{2(g)} = Mg_{(g)} + H_2O_{(g)}$ at 1473 K (1200 °C).

After the electrolysis, t_e and OCV were measured as a function of time as shown in Figure 8. There was a strong correlation between OCV and t_e. Magnesium metal dissolved in the flux near the cathode established the oxygen potential at the cathode according to the Mg/MgO equilibrium. The greater the concentration of magnesium metal in the flux near the cathode, the lower the P_{O_2}will be at the cathode. According to Eq. [16], as the P_{O_2} at the cathode decreases, the OCV will increase. Right after electrolysis, the concentration of dissolved magnesium was high leading to high t_e and OCV. However, as magnesium metal is removed from the flux by the bubbling argon gas, t_e and OCV are expected to both decrease. The OCV remained relatively constant after the electrolysis experiment, and t_e was determined to be 0.35 within two minutes after electrolysis. This high t_e indicates the presence electronic current in the flux caused by dissolved magnesium metal. After 30 minutes of bubbling the SOM electrolysis cell without applying a potential, t_e had dropped to 0.03. The decrease in t_e suggests that the dissolved magnesium metal in the flux is removed by bubbling argon gas.

The overall current efficiency based on the amount of magnesium collected compared to the total current passed was approximately 30 pct.

The overall ohmic resistance of the electrolysis cell after the electrolysis was measured to be 0.48 Ω. Since the ionic resistance of the cell is expected to remain the same before and after electrolysis, the decrease in ohmic resistance of the entire electrolysis cell can be attributed to the increase in electronic conductivity in the flux.

Figure 9(a) shows the flux microstructure, after cooling, near the cathode, along with the location of an energy dispersive spectroscopy (EDS) line scan. Figure 9(b) shows the yttrium and zirconium signal intensities in counts (cts) as a function of position in the flux. In Figure 9, the zero position begins at the cathode-flux interface. Zirconium metal was identified near the cathode, suggesting that electronic current in the flux possibly reduced the zirconia in the YSZ membrane. Importantly, no oxygen was identified near the zirconium at the cathode suggesting that the zirconium species at the cathode was in fact fully reduced zirconium metal, and not zirconia.

B. *Inert Anode Current Collector*

Table IV displays details from an isolated stirring tube cathode experiment in which an inert anode current collector was used. The design shown in Figure 4 was used. In an industrial scale SOM process, an inert anode current collector will be desirable since it will produce oxygen as a valuable byproduct at the anode. The details of an inert anode current collector are discussed in other work.[36]

Electrolysis was performed at 2.4 to 2.6 V for 16 hours in total passing 39,420 C. Periodically, the electrolysis was halted and the electronic transference number in the flux was measured. It was seen that initially, the t_e was low (0.048) and the current efficiency was high (90 pct) but with continued electrolysis, the efficiency decreased and the electronic transference number increased until the flux reached the solubility limit for magnesium dissolution; see Figure 10. This finding supports the previous discussion that as more magnesium metal was produced, t_e increased due to increasing magnesium metal dissolution in the flux. The increasing t_e with electrolysis time also correlated well with the decreasing CE during this experiment. t_e after 4 hours of electrolysis and 9,877 coulombs passed was found to be lower than when the crucible wall was used as the cathode (2 hours of electrolysis and 13,987 coulombs passed); the reasons for this are twofold 1) significantly reduced cathode area with the isolated stirring tube reduces the rate of magnesium reduction and 2) localized argon stirring at the isolated cathode removes magnesium vapor from the flux. After 31,721 coulombs were passed with the isolated stirring tube cathode during electrolysis, t_e was measured to be 0.5 and the current efficiency at this point was also measured to be between 40 and 60 pct.

C. *Reduced Total Pressure Electrolysis*

Table V shows electrolysis details from the reduced total pressure SOM experiment. The first PDS is shown in Figure 11. The dissociation potential of MgO to produce $Mg_{(g)}$ was observed at approximately 1.02 V, close to the absolute value of the standard Nernst potential (1.36 V) for the reaction $MgO + H_{2(g)} = Mg_{(g)} + H_2O_{(g)}$ at 1473 K (1200 °C). Table VI shows t_e before any electrolysis and after each of the three electrolyses performed in the low-pressure experiment. t_e remained relatively

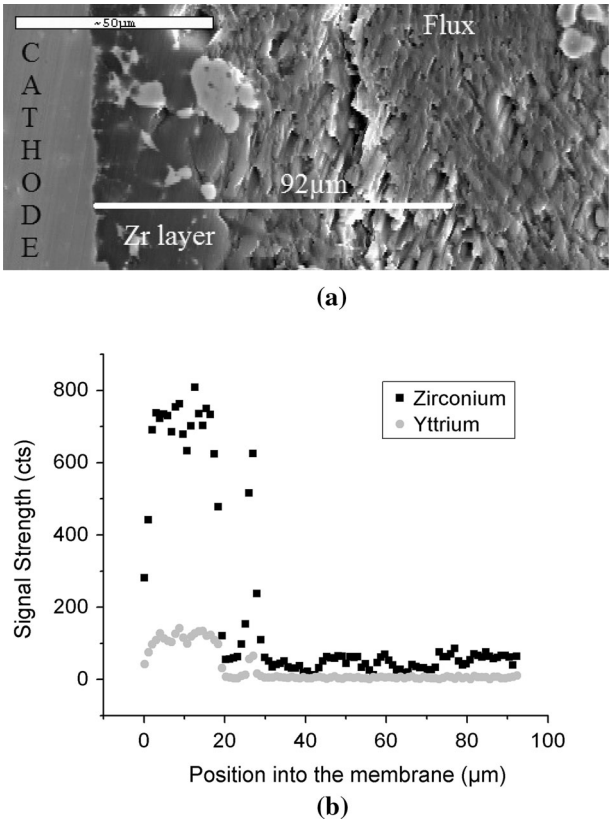

Fig. 9—(*a*) Flux microstructure near cathode and line scan location. (*b*) Yttrium and zirconium concentrations as a function of position across the flux.

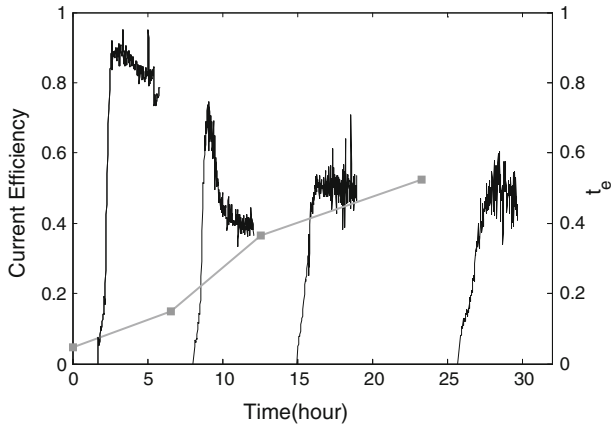

Fig. 10—During electrolysis, the current efficiency (black curve) decreases as the magnesium dissolves in the flux and the electronic transference number (gray square) increases. The asymptotic behavior indicates that the flux reaches the solubility limit for magnesium dissolution.

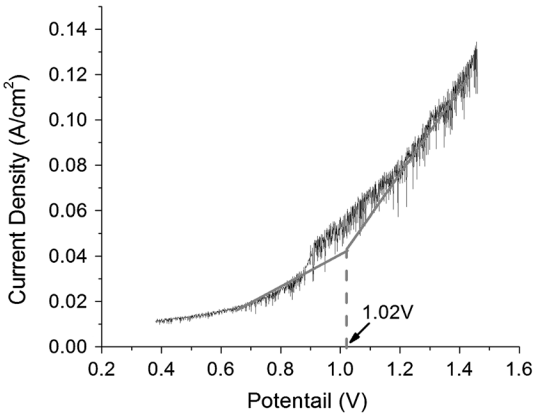

Fig. 11—Initial PDS during reduced total pressure experiment. Two MgO dissociation potentials were observed.

Table VI. t_e and Pressure After Electrolysis

	Before Electrolysis	Electrolysis 1	Electrolysis 2	Electrolysis 3
t_e	0.05	0.04	0.05	0.08
Pressure	0.08	0.08	0.08	0.24

constant through the second electrolysis at a low value. After the third electrolysis, t_e increased slightly, but still remained low relative to the other experiments described in this paper. The reason for the slight increase in t_e with the third electrolysis is described in the next paragraph.

Before the third electrolysis scan, the total pressure was increased from 0.08 to 0.24 atm. After the electrolysis scan, the t_e was measured to be 0.08. The increase in t_e is believed to be due to increase in dissolved magnesium in the flux which is due to an increased in total pressure.

The overall current efficiency of the three low-pressure electrolysis experiments performed was evaluated to be at least 75 pct (based on the metal recovery in the condenser and since some magnesium may have condensed elsewhere). Thus, the low-pressure experiment represented a major increase in current efficiency when compared to the crucible wall cathode experiment. Using EDS analysis, the magnesium metal collected from the experiment was found to be pure magnesium containing less than 1 wt pct CaF_2.

A sample of flux from the reduced total pressure experiment was made to react to hydrochloric acid, and no gas evolution was recorded. This test indicated that either no metal dissolved in the flux, or the amount of metal dissolved in the flux was too small to detect. The lack of magnesium metal in the flux helps to explain the low t_e in the low-pressure electrolysis experiment.

Finally, the cathode was examined. The maximum zirconium signal intensity within 120 μm of the cathode was measured to be 60 cts. The low signal intensity compared to electrolysis with the crucible wall (800 cts) suggests that no zirconium metal was present near the cathode-flux interface which subsequently suggests that dissociation of zirconia from the YSZ membrane did not occur.

V. CONCLUSIONS

Electronic current present in the SOM process can drastically decrease process efficiency and degrade the YSZ membrane employed in the process. Dissolved magnesium metal in the flux, used as a liquid electrolyte in the SOM process, is responsible for imparting electronic conductivity on the molten flux. The electronic transference number of the flux under different SOM process operating conditions was quantified using a two stainless steel electrode technique.

During SOM electrolysis experiments, the electronic transference number was typically found to increase immediately after electrolysis due to dissolved magnesium metal in the flux. As more magnesium metal was produced, its dissolution in the flux increased and caused the electronic transference number to also increase. As electronic transference number increased, cell current efficiency was found to decrease. Further, when the electronic transference number was sufficiently high, zirconia from the YSZ membrane was dissociated leading to membrane degradation.

By decreasing the partial pressure of magnesium metal at the cathode, the current efficiency of the SOM electrolysis cell was increased. The magnesium partial pressure at the cathode was first decreased by argon bubbling and secondly by reducing the total pressure of the entire electrolysis cell. The decreased magnesium partial pressure led to a decreased concentration of magnesium dissolved in the flux and decreased the electronic transference number. When SOM electrolysis was performed at low total pressures, the electronic transference number was also low and the zirconia in the YSZ membrane did not dissociate. An overall current efficiency of at least 75 pct was achieved during low-pressure electrolysis. The reduced total pressure electrolysis shows great promise as a viable method for operating the SOM process with extremely limited electronic current and high current efficiencies over long times.

ACKNOWLEDGMENTS

This work has been supported by the National Science Foundation under Grant No. 102663 and by the Department of Energy under Grant No. DE-EE0005547. The authors would like to acknowledge helpful discussions with Dr. Soobhankar Pati. The assistance of Robert Sjostrom is also greatly appreciated.

REFERENCES

1. G. Hanko, H. Antrekowitsch, and P. Ebner: *JOM*, 2002, vol. 54, pp. 51–54.
2. T. Pollock: *Science*, 2010, vol. 328, pp. 986–87.
3. S. Das: *JOM*, 2008, vol. 60, pp. 63–69.
4. G.J. Kipouros and D.R. Sadoway: *Adv. Molten Salt Chem.*, 1987, vol. 6, pp. 127–209.
5. U.B. Pal, D.E. Woolley, and G.B. Kenney: *JOM*, 2001, vol. 53, pp. 32–35.
6. D.J. Fray: *JOM*, 2001, vol. 53, pp. 27–31.

7. A. Krishnan, X. Lu, and U. Pal: *Metall. Mater. Trans. B*, 2005, vol. 36B, pp. 463–73.
8. A. Krishnan, X.G. Lu, and U.B. Pal: *Scand. J. Metall.*, 2005, vol. 34, pp. 293–301.
9. M. Suput, R. DeLucas, S. Pati, G. Ye, U. Pal, and A.C. Powell: *Miner. Process. Extr. Metall.*, 2008, vol. 117, pp. 118–22.
10. S. Pati, M. Suput, R. DeLucas, and U.B. Pal: in *Solid Oxide Membrane Process for Calcium Production Directly from It's Oxide*, S.M. Howard, ed., EPD Congress, Warrendale, 2008, pp. 121–26.
11. A. Roan, S. Pati, S.N. Basu, and U.B. Pal, in *TMS Supplemental Proceeding: Materials Processing and Energy Materials*, Wiley, 2011, pp. 717–21.
12. Y. Jiang, J. Xu, X. Guan, U.B. Pal, and S.N. Basu: *MRS Proc.*, 2012, vol. 1493, pp. 231–35.
13. E. Gratz, S. Pati, J. Milshtein, and A. Powell: in *Magnesium Technology*, W.H. Sillekens, S.R. Agnew, N.R. Neelameggham, S.N. Mathaudhu, eds., Wiley, San Diego, 2011, pp. 2–5.
14. E. Gratz, S. Pati, J. Milshtein, and U. Pal: in *Effect of Electronic Current on the Solid Oxide Membrane (SOM) Process for Magnesium Production*, M. Moats, G. Houlachi, E. Asselin, A. Allanore, and J. Yurko, eds., Electrometallurgy, 2012, pp. 111–18.
15. E.S. Gratz, J.D. Milshtein, and U.B. Pal: *J. Am. Ceram. Soc.*, 2013, vol. 96 (10), pp. 3279–85.
16. P. Chartrand and A.D. Pelton: *Metall. Mater. Trans. A.*, 2001, vol. 32A, pp. 1385–96.
17. A. Krishnan: Ph.D. Thesis, Boston University, 2006.
18. A.W. Searcy and R.D. Freeman: *J. Am. Chem. Soc.*, 1954, vol. 76, pp. 5229–32.
19. M.B. Panish: *J. Chem. Eng. Data*, 1961, vol. 6, pp. 592–94.
20. A. Dworkin and M. Bredig: *J. Phys. Chem.*, 1971, vol. 75, pp. 2340–44.
21. J. Thonstad: *Can. J. Chem.*, 1965, vol. 43, pp. 3429–32.
22. R. Odegard, A. Sterten, and J. Thonstad: *Metall. Trans. B*, 1988, vol. 19B, pp. 449–57.
23. H. Bronstein and M. Bredig: *J. Am. Chem. Soc.*, 1958, vol. 80, pp. 2077–81.
24. G. Haarberg and J. Thonstad: *J. Appl. Electrochem.*, 1989, vol. 19, pp. 789–801.
25. A. Martin, J.C. Poignet, J. Fouletier, M. Allibert, D. Lambertin, and G. Bourgès: *J. Appl. Electrochem.*, 2009, vol. 40, pp. 533–42.
26. X. Guan, P.A. Zink, U.B. Pal, and A.C. Powell: *ECS Trans.*, 2012, vol. 41, pp. 91–101.
27. X. Guan, P.A. Zink, U.B. Pal, and A.C. Powell: *Metall. Mater. Trans. B.*, 2013, vol. 44B, pp. 261–71.
28. X. Guan, U.B. Pal, and A.C. Powell: *JOM*, 2013, vol. 65, pp. 1285–92.
29. J.W. Kim, A.V. Virkar, K.Z. Fung, K. Mehta, and S.C. Singhal: *J. Electrochem. Soc.*, 1999, vol. 146, pp. 69–78.
30. T. Kawada, N. Sakai, H. Yokokawa, M. Dokiya, M. Mori, and T. Iwata: *J. Electrochem. Soc.*, 1990, vol. 137, pp. 3042–47.
31. N.A. Fried, K.G. Rhoads, and D.R. Sadoway: *Electrochim. Acta*, 2001, vol. 46, pp. 3351–58.
32. A.J. Bard and L.R. Faulkner: *Electrochemical Methods: Fundamentals and Applications*, Wiley, Danvers, 2001.
33. A.V. Virkar: *J. Power Sources*, 2005, vol. 147, pp. 8–31.
34. A.V. Virkar: *J. Electrochem. Soc.*, 1991, vol. 138, pp. 1481–87.
35. A. Roine: *HSC Chemistry*, 5.11 ed., Outokumpu Research Oy, Pori, Finland, n.d.
36. X. Guan, U.B. Pal, S. Gopalan, and A.C. Powell: *J. Electrochem. Soc.*, 2013, vol. 160, pp. F1179–86.